Loss of TXNDC12 Induces Oxidative Stress-mediated Autophagy in Glioblastoma Cell Lines

Xiaoye Wang (wangxiaoyehy@163.com)
Haiyang People's Hospital
Zhaohui Yan
Haiyang People's Hospital
Jingxi Bao
Haiyang People's Hospital
Huajian Li
Haiyang People's Hospital
Xinhua Yu
Haiyang People's Hospital

Research

Keywords: glioblastoma, TXNDC12, reactive oxygen species

Posted Date: November 10th, 2021

DOI: https://doi.org/10.21203/rs.3.rs-1039177/v1

Abstract

Redox homeostasis in glioblastoma cells is very important, but how it is maintained is still not well understood. Herein, we identified thioredoxin domain-containing protein 12 (TXNDC12) as a therapeutic target candidate which significantly maintained redox homeostasis in GBM cells. Overexpression of TXNDC12 was associated with increased tumor grade and poor prognosis in patients with glioma ($P < 0.001$), according to the analysis of expression data from the public database Cancer Genome Atlas. TXNDC12 protein levels were significantly elevated in glioblastoma compared to non-tumor brain tissue samples by immunohistochemistry and western blot analysis. Knockdown of TXNDC12 inhibited the proliferation of U251 and A172 *in vitro*. On day 21 post-implantation, tumor growth inhibition was 70% in A172 with stable expression of TXNDC12 shRNA *in vivo* ($P < 0.001$). Kaplan-Meier analysis of survival data showed that the overall survival of tumor-bearing animals increased from 20.3 days (control) to 28.7 days (knockout, $P < 0.05$). These data suggest that TXNDC12 is a key mediator in redox homeostasis both *in vivo* and *in vitro*. Thus, TXNDC12 is a potential treatment target of GBM.

1. Introduction

Glioma is the most commonly diagnosed primary malignant brain tumor in adults, and 70% of them are high-grade gliomas (glioblastoma, GBM)[1]. In the clinical treatment of GBM, the median survival of patients is only 14 months despite the proven effectiveness of surgery combined with radiotherapy and chemotherpy[2]. Compared with other tumors, GBM is more sophisticated in treatment due to its high heterogeneity and high recurrence rate[3]. High redox in GBM cells is essential to maintain cell proliferation, division, and invasiveness, so it is important to explore the growth and proliferation mechanisms of GBM[4].

The redox state of tumors changes with various intracellular physiological processes, for example, cells that are proliferating need to be in a reduced state more than differentiated cells; changes in the intracellular redox environment are important for either the cell cycle or apoptosis[4, 5]. The intracellular redox state is mainly determined by intracellular redox coenzymes such as NAD(P)H-NAD(P) and reduced glutathione oxidized glutathione (GSH-GSSG) concentrations. Also, thioredoxin and its related proteins are disulfide bond reductases that maintain the intracellular redox state[6-8].

Thioredoxin domain-containing protein 12 (TXNDC12) is a protein with oxidase activity encoded by the TXNDC12 gene, which is a member of the thioredoxin superfamily[9, 10]. TXNDC12 plays a key role in maintaining the intracellular reduction state, and its presence promotes the growth, migration, and invasion of hepatocellular carcinoma and gastric cancers[9]. However, information about the effect of TXNDC12 on GBM is unclear and awaits to be studied[11, 12].

To further reveal the role of TXNDC12 in the development of GBM, in this study, we use the Chinese Glioma Genome Atlas (CGGA) database, the brain tumor molecular database (Rembrandt), and The Cancer Genome Atlas (TCGA) to analyze the function of TXNDC12. The relationship between TXNDC12

and GBM grade and the patient prognosis was also investigated and analyzed by the gene knockdown technique. We found that TXNDC12 may promote the proliferation of GBM by facilitating the conversion of cells from the oxidized to the reduced state.

2. Results

2.1 *TXNDC12* is overexpressed in human gliomas and is associated with a poor prognosis

To investigate the role of TXNDC12 in human gliomagenesis, we first analyzed the mRNA levels of this gene in human glioma samples using publicly available datasets from the TCGA database. TXNDC12 mRNA levels were elevated in low grade (WHO II; n = 226) and high-grade gliomas (WHO IV, n = 150; $p < 0.0001$) compared to non-neoplastic samples (n = 4, Figure 1A). TXNDC12 expression was markedly higher in oligodendrogliomas, mixed gliomas, astrocytomas, and GBM than in non-tumor tissues. Rembrandt database results showed significant differences in TXNDC12 expression in WHO classes II, III, and IV, and the expression of TXNDC12 increased obviously with the increase of pathological grade (Figure 1B). CGGA database also indicated that TXNDC12 mRNA levels were increased in high-grade gliomas (Figure 1C).

Among all pathological types, GBM is the most malignant and has the worst prognosis. It has been demonstrated that the degree of infiltration of tumor microenvironmental cells, immune cells, and stromal cells may have an important impact on the prognosis of GBM, so we evaluated the differences in TXNDC12 expression between the classic, mesenchymal and anterior neurological types. The findings from the CGGA database analysis suggested that TXNDC12 had the highest expression in the classic GBM, followed by the mesenchymal type, and the lowest expression was in the anterior neurological type (Figure 1D). There was no apparent difference between the results of the Rembrandt database analysis and CGGA analysis, and the variation between pathological types was more evident (Figure 1E). The TCGA database told us that the differences among classic, mesenchymal, and anterior neurological types were not statistically significant, but TXNDC12 expression was higher in the mesenchymal type and statistically different from the anterior neurological type (Figure 1F).

To discuss the potential role of TXNDC12 expression in the survival of glioma patients, we generated Kaplan-Meier survival curves according to the CGGA database, Rembrandt database, and TCGA database. There was a noticeable difference between the high and low TXNDC12 expression groups, patients with a low expression of TXNDC12 had a longer survival time compared to the patients with a high level of TXNDC12 expression (Figure 1G, Figure 1H, Figure 1I, $p < 0.001$).

2.2 Immunohistochemical staining and Western blot revealed increased expression of TXNDC12 in glioma samples and cell lines

Immunohistochemical (IHC) staining of 60 paraffin-embedded clinical glioma specimens, including grade II (18 cases), grade III (18 cases), grade IV (18 cases), and non-tumor brain tissue specimens (6 cases), showed that TXNDC12 expression increased with tumor grade (Figure 2A, 2B). Also, we analyzed other

tumor-related factors, such as age, gender, tumor size, liquefactive necrosis, preoperative tumor edema, and tumor grade. The results showed that TXNDC12 expression was positively correlated with tumor grade and liquefactive necrosis, independent of age, gender, tumor size, and edema, suggesting that TXNDC12 may be a potential diagnostic marker for patients with glioma (Table 1, $p < 0.001$).

Finally, analysis of western blot results showed that TXNDC12 protein levels were also elevated in human glioma cells U87MG, U251, T98, LN229, and A172 compared to human astrocytes (NHA) (Figure 2C, 2D). Taken together, these results suggest that TXNDC12 may play an important role in both glioma development and progression, and therefore TXNDC12 could be used as a new diagnostic protein marker.

Table 1 Correlations of TXNDC12 expression with clinicopathological features in glioma patients.

Variables	n	TXNDC12 expression		*P*-value
		Low	High	
Age (year)				
<60	37	16	21	0.887
≥60	17	7	10	
Gender				
Male	29	13	16	0.951
Female	25	11	14	
Tumor size (cm)				
< 4	18	7	11	0.697
≥4	36	16	20	
Liquefactive necrosis				
Negative	35	18	17	0.305
Positive	19	7	12	
Edema				
None to mild	16	8	8	0.369
Moderate to severe	38	14	24	
WHO grade				
II	18	15	3	<0.001
III	18	5	13	
IV	18	2	16	

2.3 Knockdown of TXNDC12 suppresses the viability of glioma cells

First, we designed and synthesized two independent small interfering RNAs (si-TXNDC12-1 and si-TXNDC12-2) and tested the knockdown efficiency on TXNDC12 *in vitro*. In the U251 cell line, the knockdown efficiency of si-TXNDC12-1 was 89.3% and that of si-TXNDC12-2 was 85% (Figure 3A). In the A172 cell line, the knockdown efficiency of si-TXNDC12-1 was 88.3% and that of si-TXNDC12-2 was 79.3% (Figure 3B). As the western blot results showed, the protein level of TXNDC12 was also visibly

reduced after interfering with *TXNDC12* mRNA expression, moreover, the efficiency of si-TXNDC12-1 was slightly higher than that of si-TXNDC12-2 (Figure 3C, Figure 3D).

To verify the effect of TXNDC12, we performed cell viability assays on U251 and A172 cells with knockdown of TXNDC12. Compared with the control group, cell viability was greatly inhibited with the prolonged knockdown of TXNDC12. After 72h, the inhibition rate of cell activity was 39.5% for si-TXNDC12-1 and 24.5% for si-TXNDC12-2. The inhibitory effect of si-TXNDC12-1 was dramatically higher than that of si-TXNDC12-2 (Figure 3E). Similar experimental results were shown in the A172 cell line, with 35.8% inhibition of cellular activity for si-TXNDC12-1 and 28.3% for si-TXNDC12-2 after 72 h (Figure 3F).

2.4 Knockdown of TXNDC12 Inhibits glioma cells proliferation

For further investigation of the mechanism associated with the inhibition of cell activity, we performed phenotypic experiments related to the knockdown of TXNDC12. As shown in the EdU experiments, the number of cells in the proliferation phase (red fluorescence) was declined after the knockdown of TXNDC12 in U251 cells (Figure 4A), and the number of proliferating cells decreased from 27.7% to 10.7% (Figure 4B). Similarly, in the A172 cell line, cell proliferation was also found to be significantly inhibited after knockdown of TXNDC12, with the number of cell proliferation decreasing from 30.7% to 12.0% (Figure 4C, 4D). The results of the clone formation assay showed that the number of clonal colonies decreased and the size of clonal colonies became smaller after knockdown of TXNDC12 (Figure 4E), with a decrease in the total clonal area of about 54.5% in the U251 cell line and about 49.9% in the A172 cell line (Figure 4F).

2.5 Knockdown of TXNDC12 causes an increase in intracellular reactive oxygen species

Excessive production of reactive oxygen species (ROS), such as hydrogen peroxide (H_2O_2), superoxide radicals (O^{2-}) and highly cytotoxic hydroxyl radicals (-OH), as well as the decreased ability of cells to scavenge ROS are the main causes of intracellular oxidative stress. Since hydrogen peroxide is produced by superoxide, superoxide levels can indirectly respond to hydrogen peroxide levels. We used the fluorescent superoxide probe (dihydroethidium, DHE) to study superoxide levels. si-TXNDC12-1 transfected A172 and U251 cells showed significantly higher fluorescence intensity than the control, which was approximately 2-fold elevated (Figure 5A, 5B). Similarly, the level of H_2O_2 in cells transfected with si-TXNDC12-1 was 1.8-fold higher than that in the control group, and H_2O_2 was significantly reduced after the application of hydrogen peroxide scavenger (N-acety1-L-cysteine Figure 5C). The ROS fluorescence probe results showed that the green fluorescence intensity of si-TXNDC12-1 transfected cells was approximately 1.85-fold higher than that of the control group (Figure 5D, 5E). The above results suggest that TXNDC12 may play an important role in scavenging intracellular ROS to maintain the balance of intracellular redox reactions.

2.6 Knockdown of TXNDC12 suppresses the growth of GBM cells *in vivo*

To examine the effect of TXNDC12 on tumor growth in vivo in tumor-bearing nude mice, we implanted luciferase-expressing A172-sh-TXNDC12-1 and A172-NC cells into the brains of nude mice (10 mice per group). Tumor growth was continuously monitored over 21 days using a bioluminescence assay. By day 14, the bioluminescence values of the two groups of animals were significantly different (Figure 6A). On day 21 post-implantation, the mean volume of A172-sh-TXNDC12-1 tumors was reduced by approximately 65% compared to the NC group ($P < 0.01$; Figure 6 B). Kaplan-Meier analysis showed that the overall survival of tumor-bearing animals increased from 20.3 days (control group) to 28.7 days (knockdown group, $P < 0.05$; Figure 6C). Histological examination revealed that A172-sh-TXNDC12-1 tumors were smaller than NC tumors, and A172-sh-TXNDC12-1 tumor cells underwent significant apoptosis. There was less cell division in the tumor tissue (Figure 6D). In conclusion, these findings suggest that the downregulation of TXNDC12 inhibits the growth of GBM tumors in vivo.

3. Discussion

Despite breakthroughs in basic glioma research over the past decades, the median patient survival is less than 15 months[13-15]. The development of chemotherapeutic drugs for glioma has been slow, mainly due to the lack of ability of most drugs to be delivered across the blood-brain barrier and the fact that increasing drug doses can have significant side effects on patients' somatic functions, while the application of chemotherapeutic drugs can also enhance drug resistance in glioma[2, 16, 17]. Therefore, exploring the mechanisms related to the biological behavior of glioma cells and finding new targets for glioma therapy are expected to provide new directions for the treatment of glioma.

The TXNDC12 gene encodes a member protein of the thioredoxin superfamily[12, 18]. The main feature of this family member is that it has a thioredoxin-folding active motif that catalyzes the formation and isomerization of disulfide bonds[19, 20]. What’s more, This protein may play a role in the defense against ROS[9, 21]. In this study, a comprehensive analysis of TXNDC12 expression levels in databases and clinical glioma samples as well as the prognosis of patients showed that patients with higher TXNDC12 expression levels had higher pathological grade, higher malignancy, and worse prognosis. The results of cellular experiments indicated that TXNDC12 could promote the growth of glioma cells and TXNDC12 knockdown could significantly inhibit the growth of glioma cells.

The role of ROS in tumor therapy has received increasing attention, and various drugs that cause oxidative stress in cells by increasing ROS levels are more frequently used in clinical practice[22], but there is no uniform understanding of the role of oxidative stress in tumor therapy, especially there is no quantitative study on whether different levels of ROS in the body play an anti-cancer or pro-cancer role[23, 24]. Many drugs are used to treat tumors through oxidation, which can be broadly classified into two categories: those that increase intracellular ROS levels and induce tumor cell death, and those that inhibit the intracellular antioxidant enzyme system[25-27]. This study provides a theoretical basis for the treatment of glioma with drugs that inhibit intracellular antioxidant enzyme systems.

In GBM cells, the oxidative and antioxidant systems are maintained in a relative balance, and an increase in pro-oxidant levels or a decrease in antioxidant capacity can lead to an increase in ROS levels in vivo, resulting in a series of changes[28-31]. In this study, we further studied the mechanism of the role of TXNDC12 in regulating the proliferation process of glioma cells. TXNDC12 plays an important role in maintaining this balance. When TXNCD12 expression is inhibited, the ROS content in glioma cells is significantly increased, leading to apoptosis. In summary, this study demonstrated that TXNDC12 expression was significantly elevated in glioma patients and positively correlated with glioma disease grade, which means that patients with high TXNDC12 expression have a poorer prognosis. TXNDC12 not only affected the prognosis of glioma patients but also was associated with the promotion of glioma cell proliferation. This study provides more grounds for considering TXNDC12 as a therapeutic target for glioma and lays a theoretical foundation for the development and clinical application of TXNDC12-related drugs. Furthermore，this study provides a theoretical basis for the inhibition of intracellular antioxidant enzyme system drugs for the treatment of glioma and lays the foundation for the next development of chemotherapeutic drugs and targeted drugs.

4. Materials And Methods

4.1 Pathological Samples

A total of 60 patients who underwent cerebral lesion resection in the Department of Neurosurgery, Haiyang People's Hospital from January 2017 to January 2020 were selected, including 18 patients with pathological diagnosis of WHO grade II, 18 patients with pathological diagnosis of WHO grade III, 18 patients with pathological diagnosis of WHO grade IV, and 6 normal brain tissue samples from patients who underwent decompression due to cerebral hemorrhage or traumatic brain injury and had postoperative pathology confirmed as normal brain tissue. All patients had signed the informed consent forms, which were approved by the Ethics Committee of Haiyang People's Hospital.

4.2 Cells and Reagents

Glioma cell lines U251 and A172 were purchased from the Cell Resource Center, Shanghai Institutes for Biological Sciences, Chinese Academy of Sciences. Immunohistochemical secondary antibody SP reagent (SP-9001), goat anti-rabbit secondary antibody (ZB-2301), and DAB color development reagent (Zli-9032) were purchased from Beijing Zhongsun Jinqiao Biotechnology Co. Ltd. SiRNA was purchased from Shanghai Jima Pharmaceutical Technology Co. CCK-8 kit was ordered from Dongren Chemical Technology (Shanghai) Co. Cell proliferation imaging kit (EdU method) was purchased from Guangzhou Ribo Biotechnology Co. Crystalline violet was purchased from Shanghai Biyuntian Biotechnology Co.

4.3 Bioinformatics Analysis

Chinese Glioma Genome Atlas (CGGA), American Brain Tumor Molecular Database (Rembrandt), The cancer genome atlas (TCGA) were used to investigate TXNDC12 expression and prognostic differences, and the TCGA database was further analyzed for TXNDC12-related signaling pathways.

4.4 Cell Culture and Transfection

Glioma cells were cultured in DMEM medium containing 10% fetal bovine serum and placed in a constant temperature incubator at 37℃ with 5% CO2 for routine passaging. Cells were digested and passaged with 0.05% trypsin solution. Well-grown U251 and A172 cells were selected to make cell suspensions for cell counting and then passed to six-well plates. When the cells grew to 60%, 1 mL of fresh medium was replaced in each well and the blank control group and experimental group were set up simultaneously. The cells were transfected according to the lipofectamine 2000 transfection kit.

4.5 Western Blotting

After transfection for 48 h, the cells were collected, added with an appropriate amount of RIPA lysis solution, lysed on ice for 30 min, centrifuged at 12000 r/min for 5 min at 4℃, and then the supernatant (protein) was placed in a centrifuge tube and stored at -20℃ in a refrigerator. After the protein concentration was detected by the BCA method, 5× protein loading buffer was added to it, and the protein was denatured by boiling water bath for 10 min. For each group, about 40 μg samples were separated by electrophoresis on SDS-PAGE gels and transferred to PVDF membranes at 4℃. 5% skimmed milk powder was used for blocking and primary antibodies (1:1000 dilution of β-actin and TXNDC12 antibodies) were added separately overnight at 4℃. After washing with TBST for 3×5 min, the secondary antibody coupled with horseradish peroxidase (1:5000) was added and incubated at room temperature for 1 h. After TBST washing, ECL was added dropwise, developed, and finally, the grayscale values of each band were analyzed by Image J software.

4.6 Cell Viability and Proliferation Assays

Cell viability was assessed using the CCK-8 assay. U251 and A172 cells in good condition were inoculated in 96-well plates at 3000 cells/100 μL, and the cells were transfected 24 h later. Three replicates were set up for each group, and four 96-well plates were inoculated and incubated at 37℃ in a 5% CO_2 incubator. At 24h and 48h, 96-well plates were taken out separately and 10 μL of CCK-8 was added to each well. After incubation for 60 min at 37℃, the absorbance at 450 nm was measured using the enzyme-labeled instrument. Proliferation was assessed using the EdU incorporation assay. U251 and A172 cells in good cell status were inoculated in 24-well plates at 10,000 cells/500 μL, and the cells were transfected after 24 h. Two replicates were set up for each group and incubated at 37℃ in a 5% CO_2 incubator. After 48h incubation, fixation and staining were performed according to the instructions of the EdU kit, and fluorescence microscopy was applied to take pictures.

4.7 Statistical Analysis

SPSS 22.0 software was applied for statistical analysis. All measures were tested for normal distribution using the Shapiro-Wilk (S-W) method. Compliance with normal distribution was expressed as x±s. One-way ANOVA was used for the comparison of means between groups, and LSD or SNK methods were used

for two-way multiple comparisons. $p < 0.05$ was considered a statistically significant difference (two-tailed).

Declarations

Acknowledgments

This work was supported by the Department of Science & Technology of Shandong Province (2018CXGC1503).

Conflicts of interest

The authors declare that they have no conflicts of interest.

References

1 Omuro A, DeAngelis LM. Glioblastoma and other malignant gliomas: a clinical review. Jama 2013; 310: 1842-1850.

2 Zhang Y, Kong Y, Ma Y, Ni S, Wikerholmen T, Xi K *et al*. Loss of COPZ1 induces NCOA4 mediated autophagy and ferroptosis in glioblastoma cell lines. Oncogene 2021; 40: 1425-1439.

3 Simon T, Jackson E, Giamas G. Breaking through the glioblastoma micro-environment via extracellular vesicles. Oncogene 2020; 39: 4477-4490.

4 Stupp R, Mason WP, van den Bent MJ, Weller M, Fisher B, Taphoorn MJ *et al*. Radiotherapy plus concomitant and adjuvant temozolomide for glioblastoma. The New England journal of medicine 2005; 352: 987-996.

5 Pignatello JJ, Oliveros E, MacKay A. Advanced oxidation processes for organic contaminant destruction based on the Fenton reaction and related chemistry. Critical reviews in environmental science and technology 2006; 36: 1-84.

6 Sharick JT, Favreau PF, Gillette AA, Sdao SM, Merrins MJ, Skala MC. Protein-bound NAD(P)H Lifetime is Sensitive to Multiple Fates of Glucose Carbon. Scientific reports 2018; 8: 5456.

7 Penjweini R, Roarke B, Alspaugh G, Gevorgyan A, Andreoni A, Pasut A *et al*. Single cell-based fluorescence lifetime imaging of intracellular oxygenation and metabolism. Redox biology 2020; 34: 101549.

8 Westendorp MO, Shatrov VA, Schulze-Osthoff K, Frank R, Kraft M, Los M *et al*. HIV-1 Tat potentiates TNF-induced NF-kappa B activation and cytotoxicity by altering the cellular redox state. The EMBO journal 1995; 14: 546-554.

9 Yuan K, Xie K, Lan T, Xu L, Chen X, Li X *et al*. TXNDC12 promotes EMT and metastasis of hepatocellular carcinoma cells via activation of β-catenin. Cell death and differentiation 2020; 27: 1355-1368.

10 Alanen HI, Williamson RA, Howard MJ, Lappi AK, Jäntti HP, Rautio SM *et al*. Functional characterization of ERp18, a new endoplasmic reticulum-located thioredoxin superfamily member. The Journal of biological chemistry 2003; 278: 28912-28920.

11 Knoblach B, Keller BO, Groenendyk J, Aldred S, Zheng J, Lemire BD *et al*. ERp19 and ERp46, new members of the thioredoxin family of endoplasmic reticulum proteins. Molecular & cellular proteomics : MCP 2003; 2: 1104-1119.

12 Oka OB, van Lith M, Rudolf J, Tungkum W, Pringle MA, Bulleid NJ. ERp18 regulates activation of ATF6α during unfolded protein response. The EMBO journal 2019; 38: e100990.

13 Zhang Y, Fu X, Jia J, Wikerholmen T, Xi K, Kong Y *et al*. Glioblastoma Therapy Using Codelivery of Cisplatin and Glutathione Peroxidase Targeting siRNA from Iron Oxide Nanoparticles. ACS applied materials & interfaces 2020; 12: 43408-43421.

14 Kim MM, Aryal MP, Sun Y, Parmar HA, Li P, Schipper M *et al*. Response assessment during chemoradiation using a hypercellular/hyperperfused imaging phenotype predicts survival in patients with newly diagnosed glioblastoma. Neuro-oncology 2021.

15 Sachamitr P, Ho JC, Ciamponi FE, Ba-Alawi W, Coutinho FJ, Guilhamon P *et al*. PRMT5 inhibition disrupts splicing and stemness in glioblastoma. Nature communications 2021; 12: 979.

16 Agents shuttle across blood-brain barrier to treat Hunter syndrome. Nature biotechnology 2021.

17 Wang W, He H, Marín-Ramos NI, Zeng S, Swenson SD, Cho HY *et al*. Enhanced brain delivery and therapeutic activity of trastuzumab after blood-brain barrier opening by NEO100 in mouse models of brain-metastatic breast cancer. Neuro-oncology 2021.

18 Hägg S, Ganna A, Van Der Laan SW, Esko T, Pers TH, Locke AE *et al*. Gene-based meta-analysis of genome-wide association studies implicates new loci involved in obesity. Human molecular genetics 2015; 24: 6849-6860.

19 Steibel JP, Bates RO, Rosa GJ, Tempelman RJ, Rilington VD, Ragavendran A *et al*. Genome-wide linkage analysis of global gene expression in loin muscle tissue identifies candidate genes in pigs. PloS one 2011; 6: e16766.

20 Schmidt JM, Zhou S, Rowe ML, Howard MJ, Williamson RA, Löhr F. One-bond and two-bond J couplings help annotate protein secondary-structure motifs: J-coupling indexing applied to human endoplasmic reticulum protein ERp18. Proteins 2011; 79: 428-443.

21 Rowe ML, Ruddock LW, Kelly G, Schmidt JM, Williamson RA, Howard MJ. Solution structure and dynamics of ERp18, a small endoplasmic reticulum resident oxidoreductase. Biochemistry 2009; 48: 4596-4606.

22 Zheng Q, Liu X, Zheng Y, Yeung KWK, Cui Z, Liang Y *et al*. The recent progress on metal-organic frameworks for phototherapy. Chemical Society reviews 2021.

23 Liang S, Deng X, Ma P, Cheng Z, Lin J. Recent Advances in Nanomaterial-Assisted Combinational Sonodynamic Cancer Therapy. Advanced materials (Deerfield Beach, Fla) 2020; 32: e2003214.

24 Hayes JD, Dinkova-Kostova AT, Tew KD. Oxidative Stress in Cancer. Cancer cell 2020; 38: 167-197.

25 Ni K, Lan G, Lin W. Nanoscale Metal-Organic Frameworks Generate Reactive Oxygen Species for Cancer Therapy. ACS central science 2020; 6: 861-868.

26 Zhou Z, Ni K, Deng H, Chen X. Dancing with reactive oxygen species generation and elimination in nanotheranostics for disease treatment. Advanced drug delivery reviews 2020; 158: 73-90.

27 Harris IS, DeNicola GM. The Complex Interplay between Antioxidants and ROS in Cancer. Trends in cell biology 2020; 30: 440-451.

28 Da Ros M, De Gregorio V, Iorio AL, Giunti L, Guidi M, de Martino M *et al*. Glioblastoma Chemoresistance: The Double Play by Microenvironment and Blood-Brain Barrier. International journal of molecular sciences 2018; 19.

29 Tan J, Duan X, Zhang F, Ban X, Mao J, Cao M *et al*. Theranostic Nanomedicine for Synergistic Chemodynamic Therapy and Chemotherapy of Orthotopic Glioma. Advanced science (Weinheim, Baden-Wurttemberg, Germany) 2020; 7: 2003036.

30 Sharanek A, Burban A, Laaper M, Heckel E, Joyal JS, Soleimani VD *et al*. OSMR controls glioma stem cell respiration and confers resistance of glioblastoma to ionizing radiation. Nature communications 2020; 11: 4116.

31 Fack F, Tardito S, Hochart G, Oudin A, Zheng L, Fritah S *et al*. Altered metabolic landscape in IDH-mutant gliomas affects phospholipid, energy, and oxidative stress pathways. EMBO molecular medicine 2017; 9: 1681-1695.

Figures

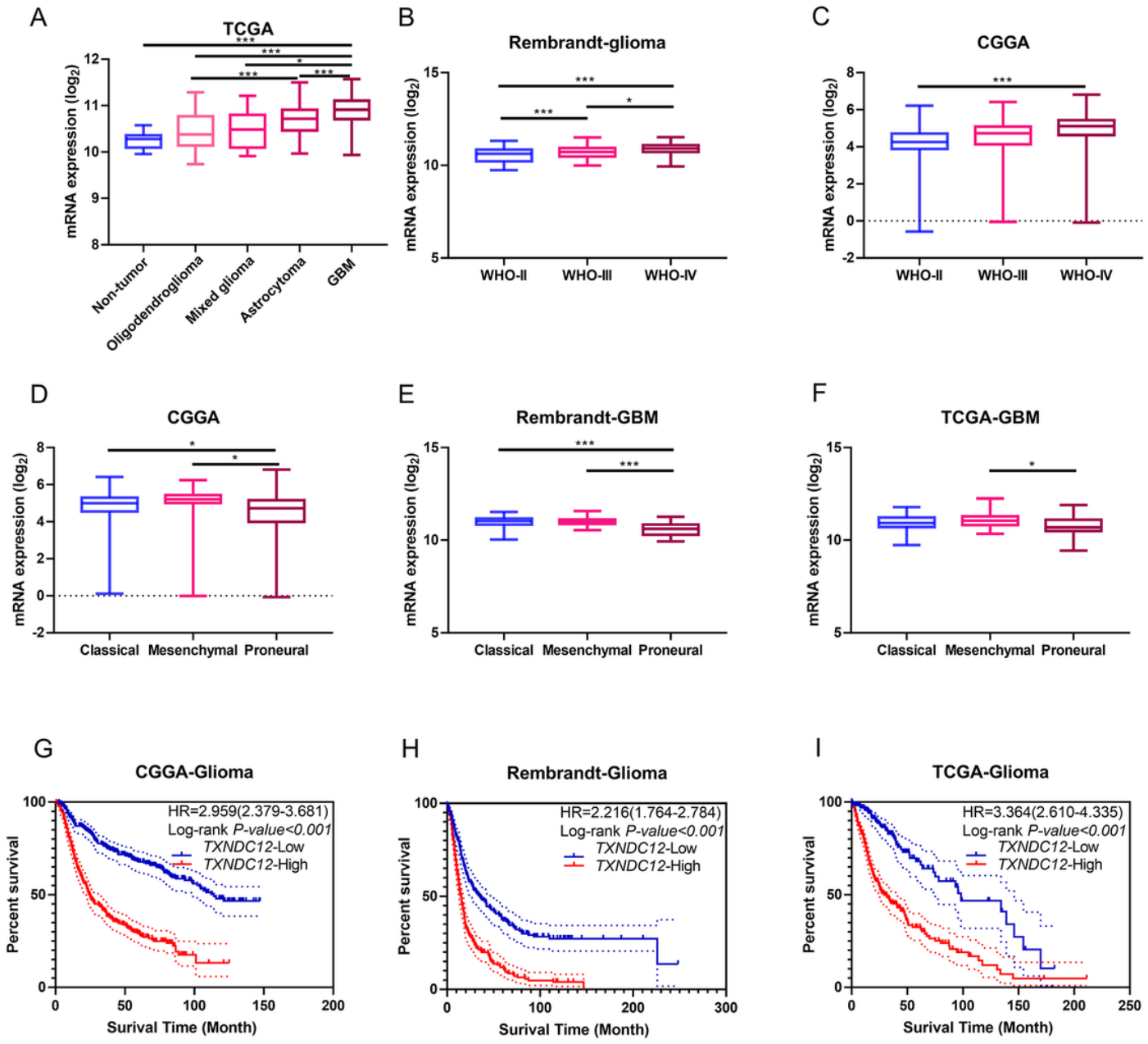

Figure 1

TXNDC12 expression is elevated in databases. (A) TXNDC12 RNA expression (log2) based on the TCGA database. (B) TXNDC12 RNA expression (log2) based on the Rembrandt database. (C) TXNDC12 RNA expression (log2) based on the CGGA database. (D) TXNDC12 RNA expression (log2) based on pathological types of CGGA database. (E) TXNDC12 RNA expression (log2) based on pathological types of Rembrandt database. (F) TXNDC12 RNA expression (log2) based on pathological types of TCGA database. (G) Kaplan-Meier survival analysis of patient overall survival data based on high versus low expression of TXNDC12 from the CGGA dataset. (H) Kaplan-Meier survival analysis of patient overall survival data based on high versus low expression of TXNDC12 from the Rembrandt dataset. (I) Kaplan-Meier survival analysis of patient overall survival data based on high versus low expression of TXNDC12 from the TCGA dataset.

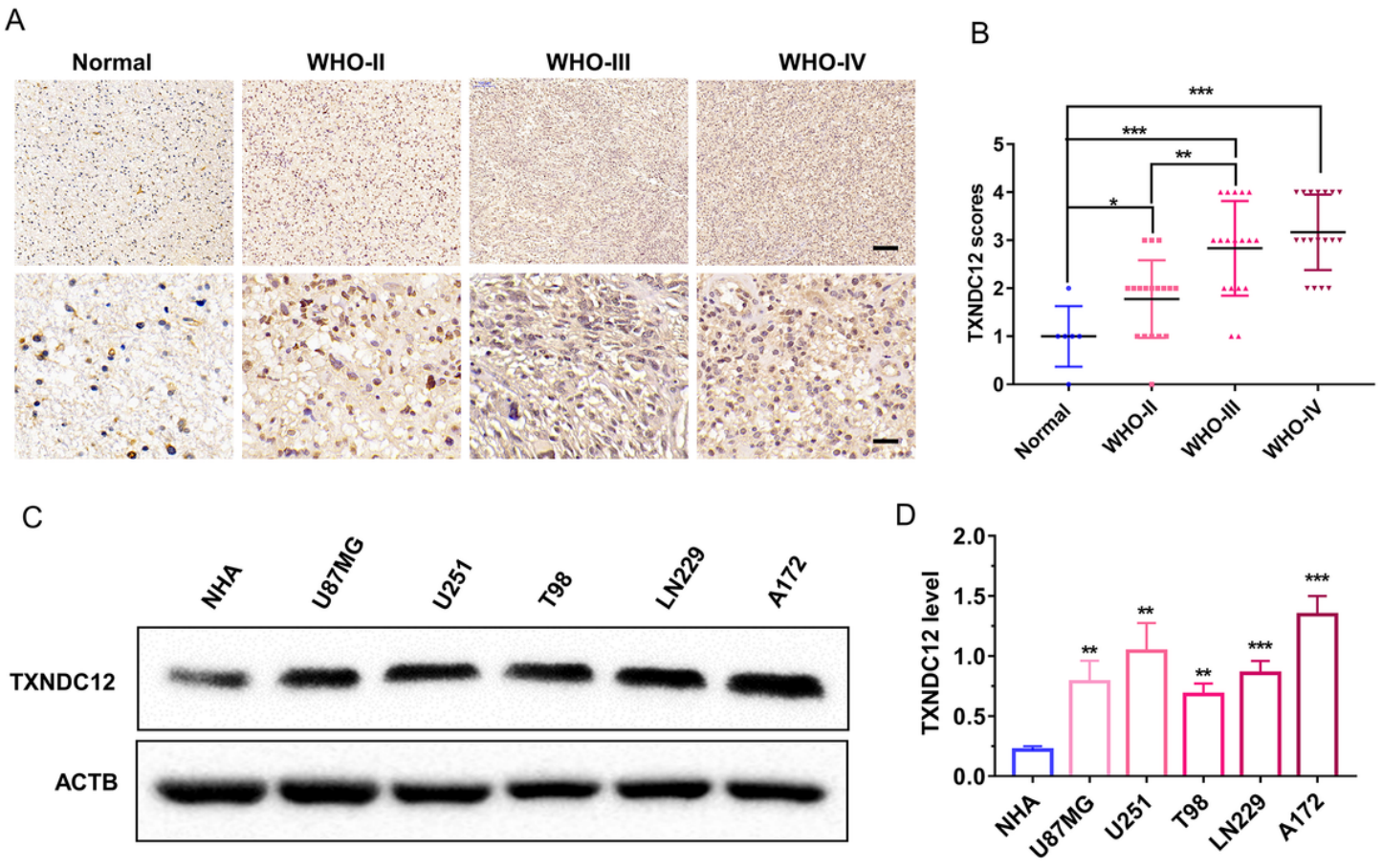

Figure 2

TXNDC12 expression is elevated in glioma samples and cell lines. (A) Representative images of IHC staining for TXNDC12 in human glioma and non-neoplastic brain tissue samples (Normal, n=6; WHO II, n = 18; WHO III, n = 18; WHO IV, n = 18). Scale bar for the upper images, 50 μm and the lower images, 100 μm. (B) Graphical results showing the IHC scores. (C) Representative western blot of TXNDC12 protein levels in normal human astrocytes (NHA) and human GBM cell lines. (D) Relative quantification of western blots shown in (C).

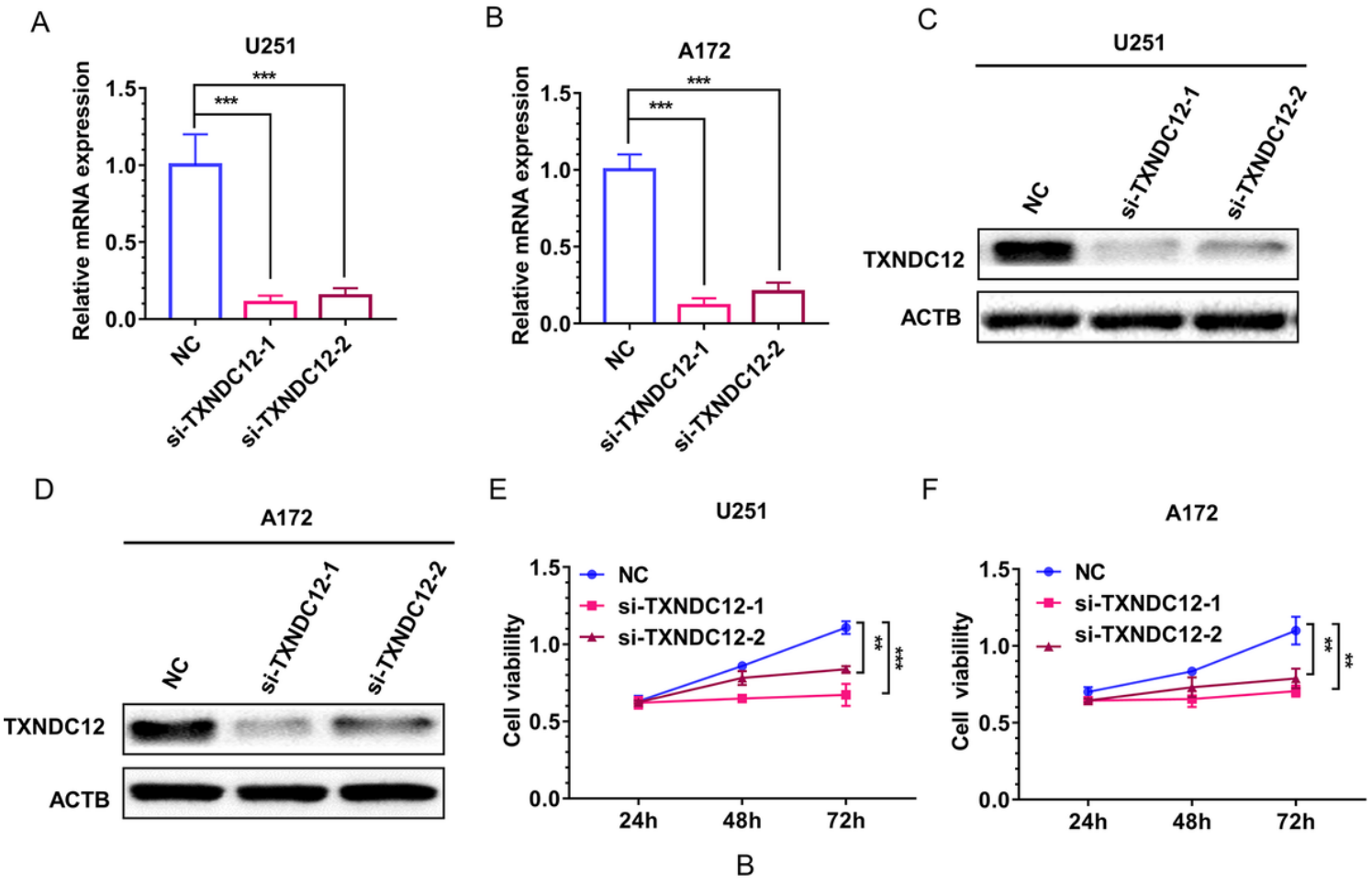

Figure 3

Silencing of TXNDC12 inhibits GBM cell viability. (A) qRT-PCR to detect TXNDC12 mRNA levels in U251 cells transfected with two independent TXNDC12 siRNAs, si-TXNDC12-1 and si-TXNDC12-2. (B) qRT-PCR to detect TXNDC12 mRNA levels in A172 cells transfected with two independent TXNDC12 siRNAs, si-TXNDC12-1 and si-TXNDC12-2. (C) Western blot analysis of TXNDC12 protein levels in U251 cells transfected with two independent TXNDC12 siRNAs, si-TXNDC12-1 and si-TXNDC12-2. (D) Western blot analysis of TXNDC12 protein levels in A172 cells transfected with two independent TXNDC12 siRNAs, si-TXNDC12-1 and si-TXNDC12-2. (E) Growth curves for si-TXNDC12 transfected U251 cells generated with OD 450 readings plotted over time using the CCK8 assay. (F) Growth curves for si-TXNDC12 transfected A172 cells generated with OD 450 readings plotted over time using the CCK8 assay.

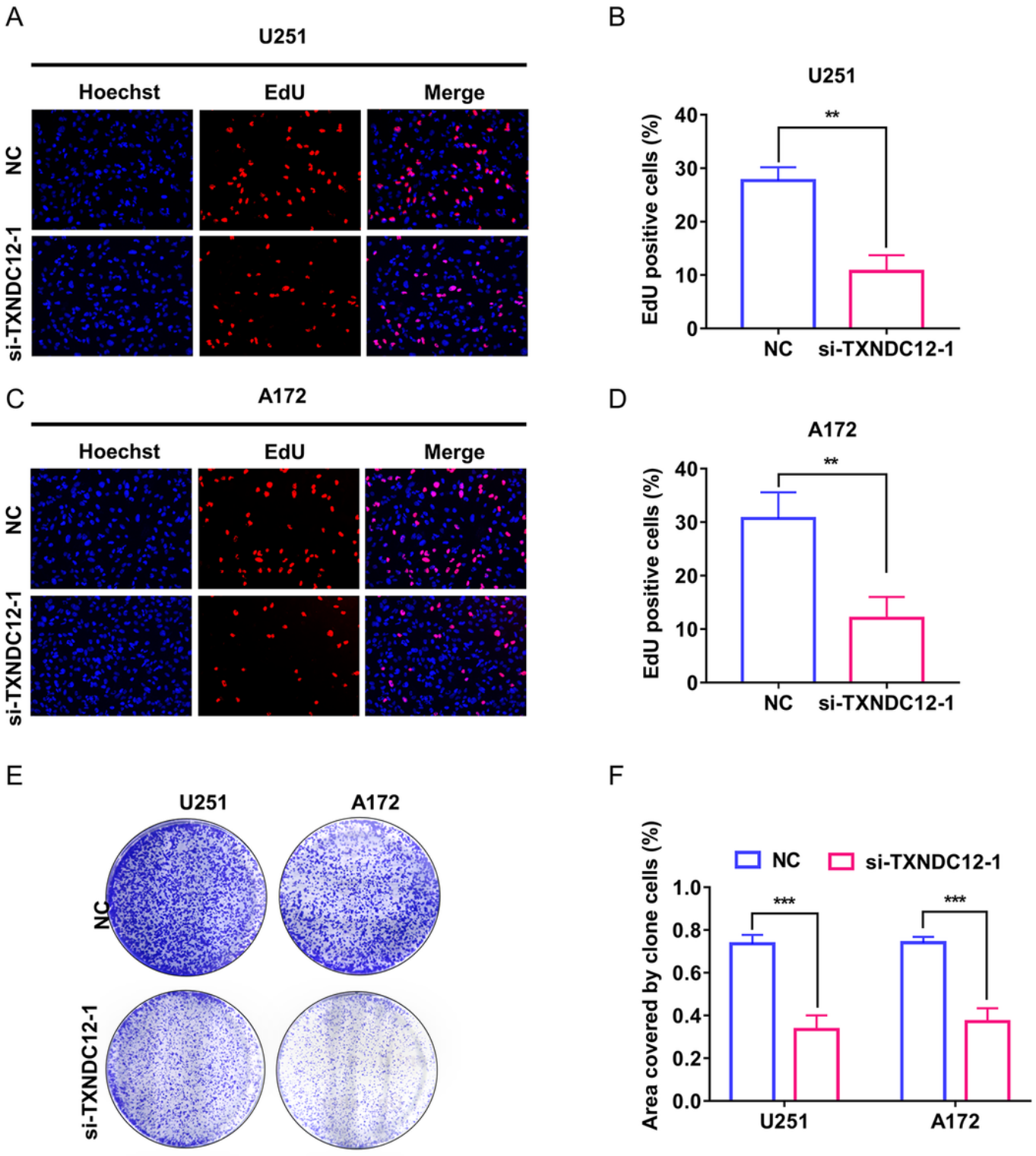

Figure 4

Knockdown of TXNDC12 Inhibits glioma cell proliferation. (A) Fluorescence images of EdU assays performed on U251 cells transfected with si-TXNDC12-1. Nuclei were stained with DAPI (blue). Scale bar, 100 μm. (B) Graphic representation of the ratios of EdU positive cells in U251 cells transfected with si-TXNDC12-1. (C) Fluorescence images of EdU assays performed on A172 cells transfected with si-TXNDC12-1. Nuclei were stained with DAPI (blue). Scale bar, 100 μm. (D) Graphic representation of the

ratios of EdU positive cells in A172 cells transfected with si-TXNDC12-1. (E) Representative images of colony-forming assays for U251 and P3-GBM cells transfected with si-TXNDC12-1 to evaluate cell proliferation. Cells were fixed and stained with crystal violet, and colonies were counted. (F) Graphic representation of the number of colonies shown in (E).

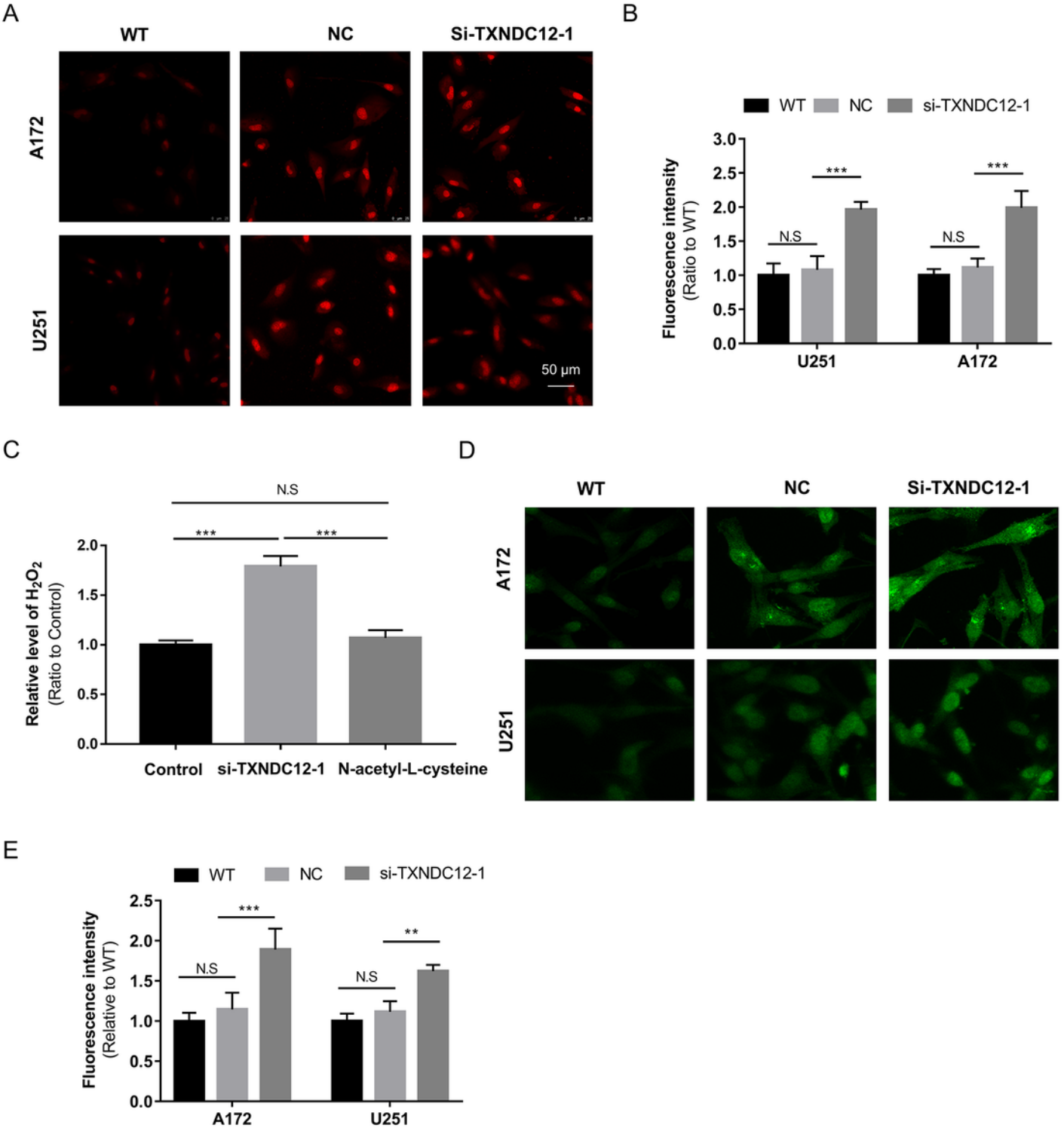

Figure 5

Intracellular reactive oxygen species increase with the loss of TXNDC12. (A) Representative images of dihydroethidium (red) superoxide probe 48 h after transfection of cells with si-TXNDC12-1. For each group of 2 cell lines, 3 images from triplicate experiments were counted. (B) Statistical analysis of the fluorescence intensities of A172 and U251 GBM cell lines transfected with si-TXNDC12-1 compared to their respective control cells. (C) H2O2 levels detected in U251 cells transfected with si-TXNDC12-1 and si-TXNDC12-2. for 48 h. (D) ROS fluorescent probe result of A172 and U251 cells transfected with si-TXNDC12-1 for 48 h. (E) Statistical analysis of the green fluorescence intensities in (D).

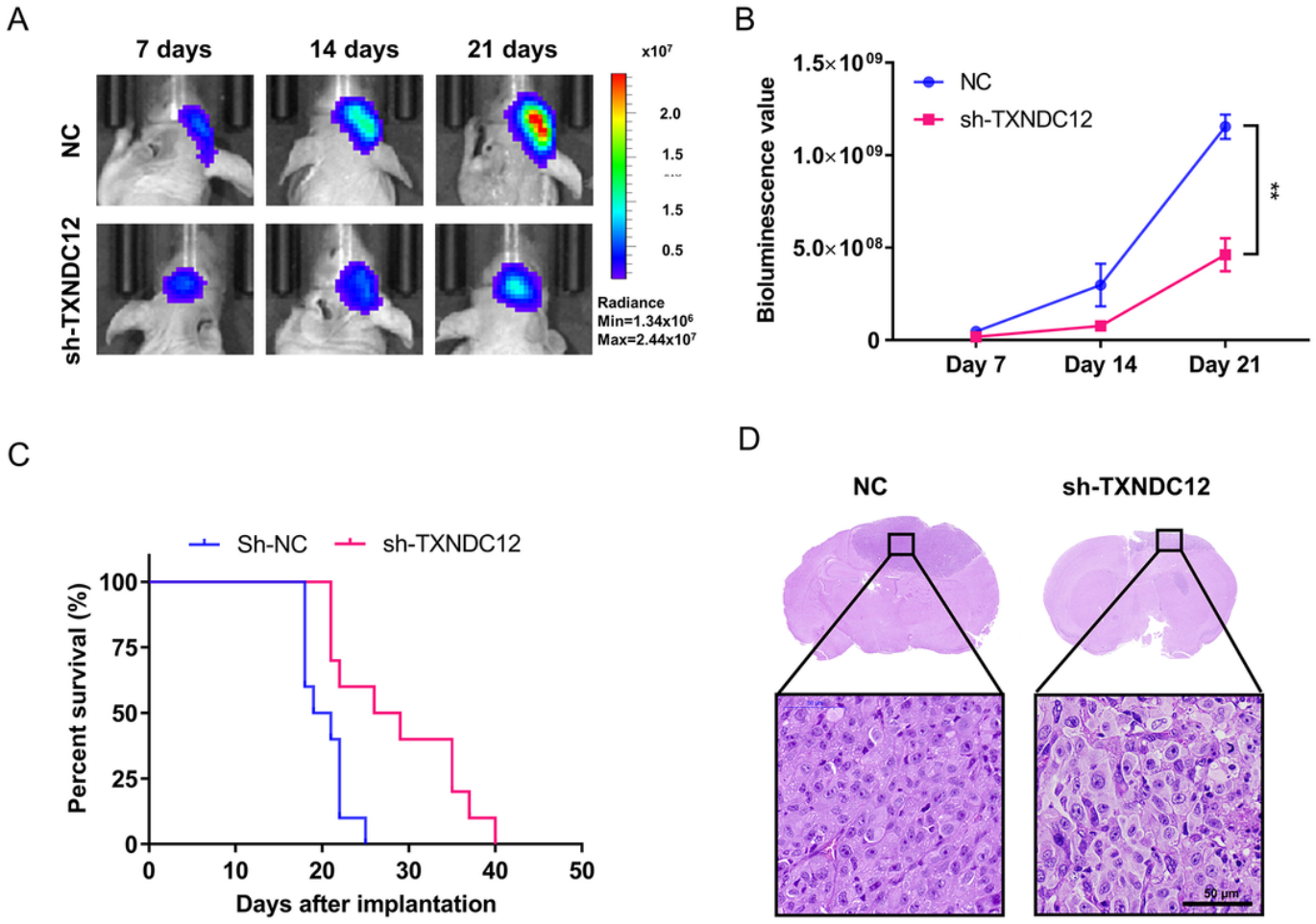

Figure 6

Down-regulation of TXNDC12 reduces in vivo tumor growth. (A) Images of Intracranial tumor growth of luciferase-expressing A172-sh-TXNDC12-1 cells or A172-NC cells monitored at days 7, 14, and 21 after implantation using the IVIS-200 imaging system to detect bioluminescence. (B) Quantification of the bioluminescent signals from the orthotopic tumors in mice implanted with A172-sh-TXNDC12-1 cells or A172-NC cells at days 7, 14, and 21. (C) Kaplan-Meier analysis of overall survival of tumor-bearing animals. A log-rank test was used to assess the statistical significance of the differences. (D) Representative images of hematoxylin and eosin-stained sections from brains of orthotopic A172-sh-TXNDC12-1 or A172-NC tumor-bearing nude mice. Scale bar, 100 μm.